Selective Arylation of Selenocysteine of Thioredoxin Reductase 1 by an Organogold Compound: Expanding the Tool-Box of Metal-Templated Reactions in Cancer Cells

Lukas Skos[1,2,†], Claudia Schmidt[3,†], Sophie R. Thomas[3], Mihyun Park[3], Riccardo Bonsignore[4], Giorgia Del Favero[5,6], Thomas Mohr[1], Andrea Bileck[1,7], Christopher Gerner[1,6,7], Angela Casini[3,*], Samuel M. Meier-Menches[1,7,8,*]

[1] *Department of Analytical Chemistry, University of Vienna, Waehringer Str. 38, A-1090 Vienna, Austria*

[2] *Doctoral School of Chemistry, University of Vienna, Waehringer Str. 38, A-1090 Vienna, Austria*

[3] *Chair of Medicinal and Bioinorganic Chemistry, Department of Chemistry, School of Natural Sciences, Technical University of Munich, Lichtenbergstr. 4, 85748 Garching, Germany*

[4] *Dipartimento di Scienze e Tecnologie, Biologiche, Chimiche e Farmaceutiche, Universitàdegli Studi di Palermo, Palermo 90128, Italy*

[5] *Department of Food Chemistry and Toxicology, University of Vienna, Waehringer Str. 38, A-1090 Vienna, Austria*

[6] *Core Facility Multimodal Imaging, University of Vienna, Waehringer Str. 38, A-1090 Vienna, Austria*

[7] *Joint Metabolome Facility, University of Vienna and Medical University of Vienna, Waehringer Str. 38, A-1090 Vienna, Austria*

[8] *Institute of Inorganic Chemistry, University of Vienna, Waehringer Str. 42, A-1090 Vienna, Austria*

[†] *These authors contributed equally*

corresponding authors:

samuel.meier-menches@univie.ac.at; angela.casini@tum.de

keywords: arylation · cancer · chemoproteomics · gold · metals in medicine · selenoprotein · thioredoxin reductase 1

ABSTRACT

Cyclometalated gold(III) complexes have been reported to template C-S cross-coupling reactions in a biological environment and acting as modifiers of cysteine residues. To broaden the scope of organogold complexes for covalent protein post-translational modification in cancer cells, an oxime-containing C^N-cyclometalated gold(III) compound was synthesised featuring a carboxylic acid group for either immobilisation on amine-bearing solid support (**Au**), or functionalisation with a fluorescent tag (**Au-Fluo**). Live-cell imaging revealed that **Au-Fluo** distributed evenly into SW480 colon carcinoma cells, with a slight preference for the nuclear and nucleolar compartments. Thioredoxin reductase 1 (TXNRD1) was observed as the major interactor of **Au** from SW480 cell lysates in chemoproteomic approaches and a 2 : 1 binding stoichiometry resulted from titration-dependent pull-downs. Direct interactions confirmed a high reactivity of **Au** towards the catalytic CysSec-dyad at the C-terminus of TXNRD1 and revealed double arylation events at this motif. Therefore, the observed **Au**-templated arylation of selenocysteine likely contributes to the compound's biological effects. Proteome profiling of SW480 cancer cells treated with sub-cytotoxic concentrations of **Au** revealed an apparent reduction of the available selenium pool by down-regulating the detected selenoproteins, except TXNRD1. Additionally, **Au** treatment induced the NRF2-KEAP1 stress response, pointing towards a disturbance of the intracellular redox balance by **Au**-mediated covalent targeting of TXNRD1. Inhibition of heme oxygenase-1 (HMOX1), the most strongly induced NRF2-target, showed pronounced synergism with **Au** treatment. Overall, organogold compounds, templating the formation of C–S(Se) bonds in cells as a novel mode of action, hold promise for the targeted modification of (onco)proteins.

INTRODUCTION

Gold-based drugs show promise as anticancer agents that are endowed with different modes of action (MoA) with respect to classical platinum-based chemotherapeutics.[1-5] Most of the known cytotoxic gold compounds have been observed to induce apoptosis in cancer cells *via* protein-targeting pathways,[6] with a few remarkable exceptions.[7,8] Recently, it has been shown that gold(III) complexes can modulate bioprocesses through metal-templated post-translational modifications of proteins, and as such emerge as new chemical tools for bioorthogonal transformations *in vitro* and *in vivo,* as well as novel drug leads.[9] For example, the anticancer gold(III) *meso*-porphyrin IX was shown to covalently modify protein cysteine thiols of thioredoxin, peroxiredoxin and deubiquitinases.[10] The gold(III) centre here is crucial to activate the *meso*-carbons of the porphyrin ring towards nucleophilic substrates. In 2017, the first *in vivo* study on a gold-activated reaction was published by Tanaka and co-workers, whereby a C^N-cyclometalated gold(III) compound, non-covalently bound to an *N*-glycoalbumin carrier and in virtue of its Lewis acid character, was capable of activating propargyl ester functions for binding to proteins by amide bond formation.[11]

Moreover, some gold(III) organometallic compounds are known to perform metal-templated covalent additions of ligands to biological nucleophiles, especially cysteine thiols.[12] In this context, we and others observed that bidentate C^N-cyclometalated gold(III) compounds, following coordination to the target amino acid residue, can template the formation of covalent aryl-peptide adducts *via* C–S cross-coupling at cysteine residues (Fig. 1A).[13-15]

For example, [Au($C^{CO}N$)Cl_2] ($C^{CO}N$ = 2-benzoylpyridine, Fig. 1B) caused cysteine arylation in model peptides, and was more reactive than other C^N-cyclometalated derivatives.[16] Interestingly, this chemistry does not work on cysteines at the *N*-terminus of peptidic domains and neither on other nucleophilic amino acids (*e.g.* lysine).[15] Activity-based proteomic profiling of [Au($C^{CO}N$)Cl_2] in *Staphylococcus aureus* cell extracts showed that the compound can efficiently arylate cysteine thiol residues of >100 proteins of which more than 50% were not engaged by the established α-chloroacetamide.[17] Out of the ligandable sites, ten potential arylation sites were assigned to be close to the respective functional protein sites; amongst the identified proteins some were already known targets for metal compounds with antibacterial effects.[17]

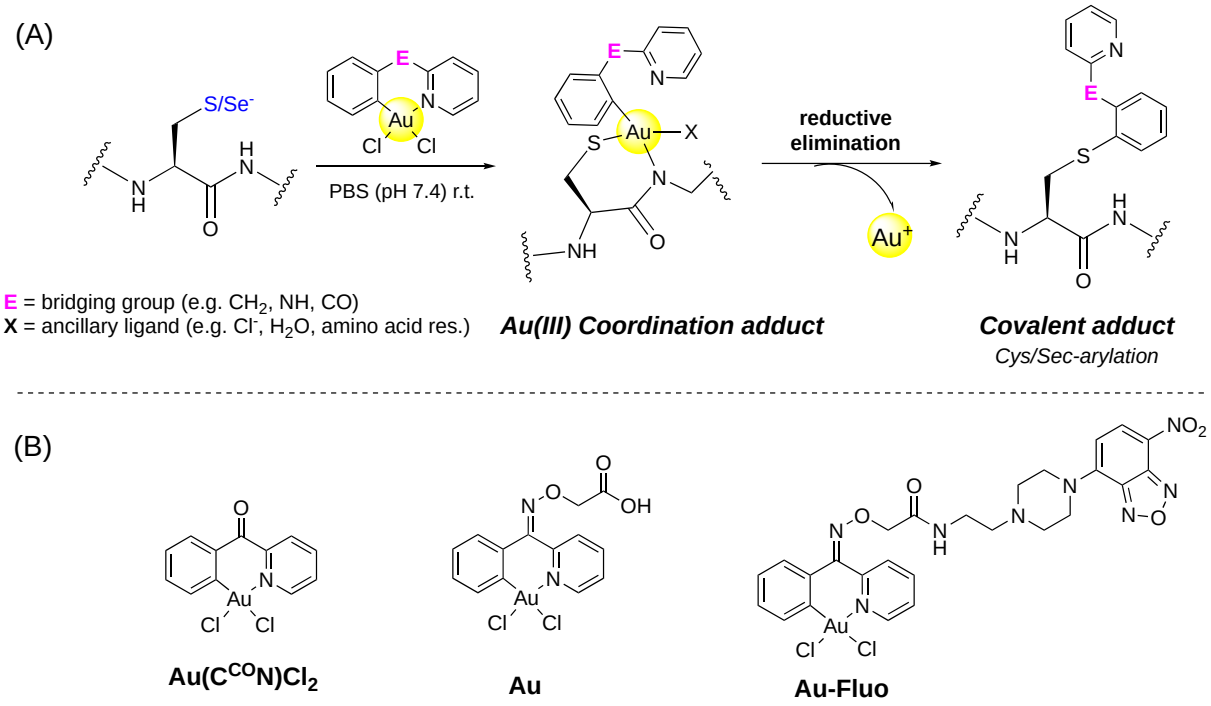

Figure 1. (**A**) Proposed scheme of the reaction of C^N-cyclometalated gold(III) compounds with thiols and selenols of proteins. The binding proceeds via two steps: *i)* the formation of a coordination adduct in which the gold(III) centre binds directly to the S^-/Se^- nucleophiles, and *ii)* arylation product forming a covalent adduct with the peptide target *via* reductive elimination. (**B**) Chemical structures of $[Au(C^{CO}N)Cl_2]$ ($C^{CO}N$ = 2-benzoylpyridine) and of the investigated C^N-cyclometalated gold(III) analogues **Au** (with a functional carboxylic acid *via* an oxime) and **Au-Fluo**.

Overall, gold(III)-templated reactions for covalent targeting of amino acid residues hold promise for anticancer applications. Furthermore, cyclometalation is one of the main strategies to stabilise gold(III) centres towards reduction, so that these compounds become sufficiently stable for medicinal applications, and can be functionalised for imaging or targeting purposes.[18,19] Therefore, we here explore a chemoproteomic approach to elucidate the protein target landscape of a C^N-cyclometalated gold(III) compound that enables metal-templated arylation of amino acids in human cancer cells. It is worth mentioning that recent years witnessed a considerable increase in mechanism-driven research in metallodrug discovery.[20-22] Mass spectrometry contributed decisively to MoA deconvolution as an enabling technology for the investigation of the reactivity of metal-based candidates[23-25] and target profiling using proteomic techniques.[20,26] Target profiling experiments were used as powerful hypothesis-generating platforms to identify protein targets of ruthenium(II/III),[27,28] rhenium(I),[29] gold(III)[30] and platinum(II)[31] candidate drugs.

In the case of the organoruthenium compound plecstatin-1, an exquisite target selectivity was evidenced for the scaffold protein plectin and its modulation by the compound mimics genetic plectin

knockout phenotypes.[32] Similarly, metalloproteomic techniques were employed to successfully characterise the chromium(III)-,[33] gold(I)-[34] and bismuth-binding proteome.[35]

The C^N-cyclometalated gold(III) complex used in this study features a functional carboxylic acid group (**Au**, Fig. 1B) that enables chemoproteomic experiments to be performed in order to track protein binding in native whole cell lysates of human SW480 colon cancer. Perturbation studies are also performed upon treating SW480 cancer cells with **Au** using proteomic profiling to characterise the cellular response to the treatment. Further, the conjugation of **Au** to a fluorescent moiety allowed us to assess the compound's intracellular distribution by live-cell fluorescence microscopy. Prior to the proteomic approaches, the reactivity of the compound in physiological conditions and in the presence of different biological nucleophiles has been studied by different methods, including ^{1}H NMR and fluorescence spectroscopy, as well as mass spectrometry. Additionally, the extent and binding sites of gold(III)-templated arylation has been characterised on relevant target proteins. Our results evidenced the selective covalent arylation of thioredoxin reductase 1 (TXNRD1) by **Au**. Notably, selective selenocysteine arylation was identified as a major contributor to the MoA of this gold(III)-lead compound. The reactivity of the unique CysSec-dyad of TXNRD1 may be responsible for the unusual target selectivity, which showed specific bis-arylation events even in the presence of other free thiols.

RESULTS & DISCUSSION

Synthesis and characterisation

In order to investigate the potential of therapeutic protein targeting *via* metal-templated covalent modification, the initial [Au($C^{CO}N$)Cl_2] complex was derivatised to an oxime-containing C^N-cyclometalated compound featuring a functional carboxylic acid group for immobilisation on amine-bearing solid support, or with a fluorescent tag (**Au-Fluo**, Fig. 1B) for investigating its intracellular accumulation and distribution by fluorescence microscopy. In general, the carboxylic acid functional group enables facile derivatisation with secondary handles *via* an amidation reaction.

The compound **Au** was synthesised according to a previously reported procedure.[33] The fluorescent derivative **Au-Fluo** was synthesised by amidation of **Au** with the 2-(-4-(7-nitrobenzo[*c*][1,2,5]oxadiazol-4-yl)piperazon-1-yl)ethane-1-amine (NPC) fluorophore, and characterised by standard analytical methods (SI, Fig. S1 and S2).

Aqueous stability and reactivity with model nucleophiles

To test the stability and hydrolysis of the complexes **Au** and **Au-Fluo**, they were dissolved in DMSO-d_6 : D_2O (9 : 1) and analysed by ^{1}H NMR spectroscopy (SI, Fig. S3 and S4). The compounds were stable over 24 h under these conditions, as suggested by the observation of the characteristic doublet at 9.31 ppm for **Au** and **Au-Fluo**, corresponding to the proton adjacent to the Au-N bond in the pyridinyl ring (α-H).

Additionally, both compounds were investigated with respect to their ability to arylate thiols as observed for [Au($C^{CO}N$)Cl_2]. The compounds were incubated in the same setting as the hydrolysis studies but in the presence of 3 equiv. of *N*-acetylcysteine (NAC, Fig. 2 and SI, Fig. S5).

The characteristic shift of the ^{1}H-NMR signal of α-H corresponding to thiol arylation[13] was observed from 9.3 ppm to 8.5 ppm for both **Au** and **Au-Fluo**. The kinetics of C-S bond formation varied only slightly among the three compounds, with **Au** inducing complete arylation within the timescale of the first measurement (time = 0), as also seen for [Au($C^{CO}N$)Cl_2] (SI, Fig. S6), whereas **Au-Fluo** required a few extra minutes.

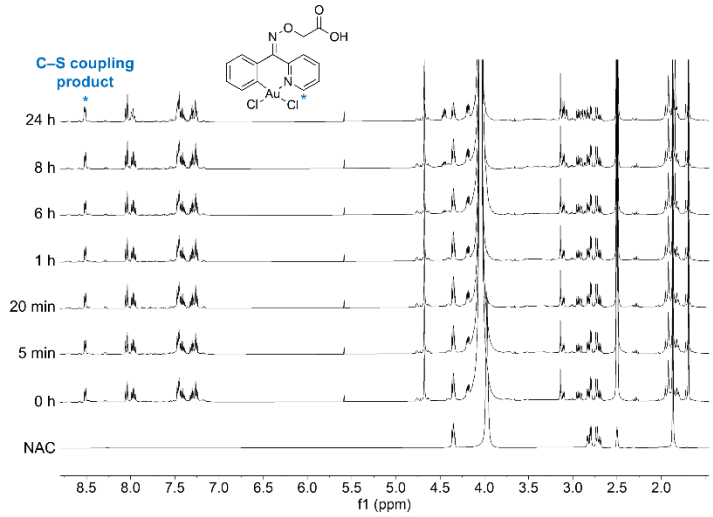

Figure 2. Reactivity of Au towards *N*-acetylcysteine (NAC). ^{1}H-NMR spectra of **Au** reacting with 3 equiv. of *N*-acetylcysteine (NAC) in DMSO-d_6 : D_2O (9 : 1). The spectrum of NAC alone is included as a reference. The characteristic shift of the α-H was observed (Δ = 0.78 ppm), indicating a rapid C-S coupling of **Au** with NAC.

The interaction of **Au-Fluo** with bovine serum albumin (BSA) was studied by fluorescence spectroscopy. First, the luminescence properties of the compound were determined (Fig. 3A). For the study with BSA, 1 equiv. of **Au-Fluo** and 10 equiv. of BSA were dissolved in PBS (pH 7.4) : DMSO (9 : 1) and incubated

at 37 °C for 1 h and 24 h. As controls, solutions of **Au-Fluo** and BSA at the same concentrations were measured under the same conditions. The fluorescence emission spectrum of **Au-Fluo** features a maximum at 557 nm, which, upon formation of the gold compound-protein adduct after 1 h of incubation, undergoes a blue shift of approx. 10 nm towards 547 nm (Fig. 3B). Most notably, the fluorescence intensity further increases by approx. 60% over 24 h, indicative of adduct formation.

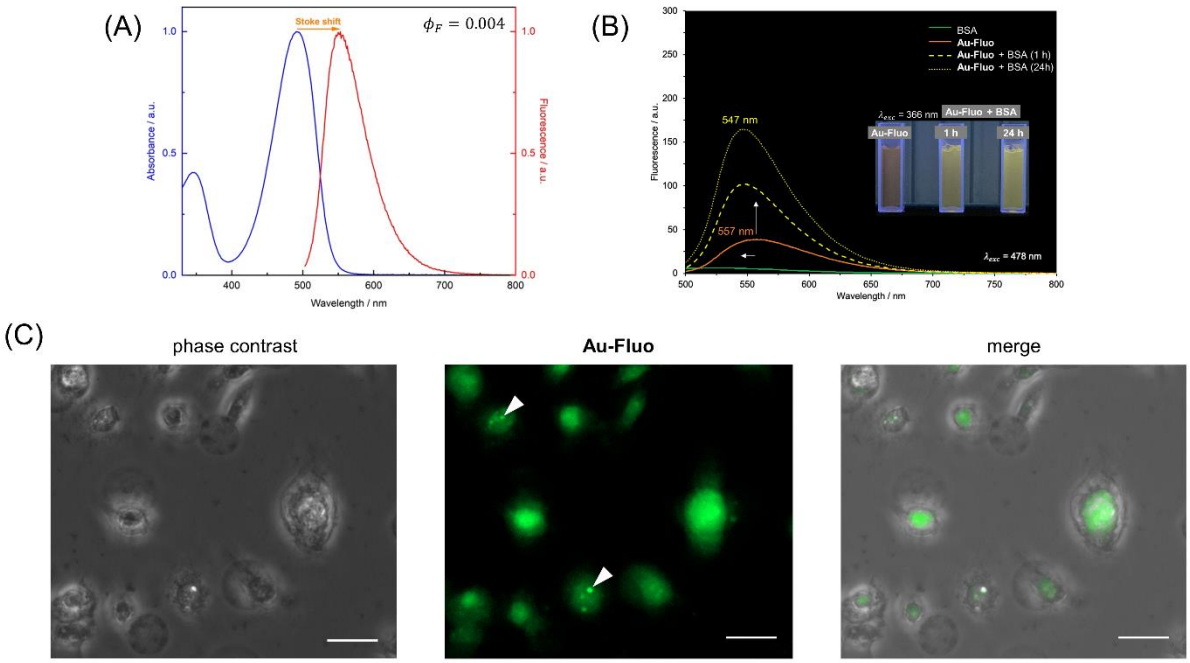

Figure 3. Fluorescence spectroscopy and microscopy studies of Au-Fluo. (**A**) Absorbance (blue, $\lambda_{abs,max}$ = 493 nm) and emission (red, $\lambda_{em,max}$ = 553 nm) spectrum of **Au-Fluo** in DMSO with the related Stokes shift (orange) of $\Delta\lambda$ = 62 nm, and the calculated fluorescence quantum yield (ϕ_F). For the emission spectrum, **Au-Fluo** was excited at the absorbance maximum of 493 nm. (**B**) Fluorescence emission spectra recorded over time of the interaction between **Au-Fluo** (1 equiv.) and bovine serum albumin (BSA, 10 equiv.) at an excitation wavelength of 478 nm. Spectra were recorded in PBS (pH 7.4) : DMSO (9 : 1) and samples were incubated at 37 °C for 1 h and 24 h. The spectra of BSA (green) and free **Au** (red) incubated for 24 h are also reported for comparison. (**C**) Cellular distribution of **Au-Fluo** in SW480 cancer cells after 4 h incubation studied by live-cell fluorescence microscopy. Green fluorescence was monitored after excitation at 469 nm and emission at 525 nm (GFP channel). The scalebar indicates 25 µm.

Antiproliferative activity and cellular distribution

The antiproliferative activity of the two compounds **Au** and **Au-Fluo** was determined in human SW480 colon cancer cells using the colorimetric MTT assay. Cells were incubated for 24 h and 72 h with

the respective compounds at different concentrations. Overall, the compounds showed moderate cytotoxic effects. The half-maximal effective concentration (EC_{50}) for cell growth inhibition was determined to be 62 ± 1 µM and 32 ± 6 µM for **Au** and **Au-Fluo**, respectively, after 24 h. After 72 h, the potency increased slightly to EC_{50}-values of 31 ± 9 µM for **Au** and 20 ± 2 µM for **Au-Fluo**.

The luminescence properties of **Au-Fluo** were further used to track its cellular distribution in SW480 cancer cells by live-cell fluorescence microscopy. The emission spectrum of **Au-Fluo**, featuring an excitation maximum at 493 nm and an emission maximum at 553 nm in PBS : DMSO (9 : 1), enabled excitation at 469 nm and data acquisition by green fluorescence. For cellular accumulation studies, the cells were treated with **Au-Fluo** at half EC_{50} concentration (16 µM) for up to 24 h. In order to reduce the background fluorescence, the medium was exchanged before analysis. The images in Fig. 3C after 4 h incubation show that **Au-Fluo** accumulates and distributes evenly into SW480 cancer cells with a slight preference for the nuclear compartment and nucleoli (arrow-heads). This distribution remained similar up to 24 h.

Target identification in SW480 cancer cells

Since the parent compound [Au($C^{CO}N$)Cl_2] was shown to chemoselectively arylate a number of cysteine thiols in bacteria, we aimed to evaluate the **Au**-mediated cysteine arylation capability in the proteome of SW480 cancer cells using a chemoproteomics approach.[20,27] First, the coupling conditions of the carboxylate-containing **Au** to the sepharose resin containing amine functional groups were optimised. The amidation reaction turned out to proceed selectively in an aqueous solution in the presence of 1.5 equiv. of 1-ethyl-3-(3-dimethylaminopropyl)carbodiimide (EDC) at pH 4 when using **Au** and 1 equiv. of serotonin as a model amine. The reaction required at least 18 h to proceed, which led to the hydrolysis of one chlorido ligand and the formation of a gold(III)-hydroxido complex upon amidation, as detected by ion trap mass spectrometry at *m/z* 661.11 (m_{theor} = 661.09) with a characteristic single chloride isotope pattern (SI, Fig. S7). Subsequently, the same conditions for immobilising **Au** on amine-containing sepharose resins were employed.

However, in this case, a 3-fold excess of **Au** with respect to the available amines was used to increase the efficiency of coupling. The chemoproteomic experiment was performed in a differential approach

(Fig. 4A): The immobilised **Au** on sepharose resin was exposed to a native protein whole cell lysate of SW480 cancer cells for 2 h. During this time, immobilised **Au** coordinates to nucleophiles under competitive conditions. Chemoselective arylation of biological nucleophiles occurs by reductive elimination and release of Au(I)/Au(0). Interacting proteins are thus irreversibly bound to the resin. This pull-down also yields non-selective binding of proteins to the resin due to hydrophobic interactions. To account for the latter, a separate competitive pull-down experiment was performed, where the native whole cell lysate was pre-incubated for 2 h with free **Au** (12 µM) and then incubated for another 2 h with the **Au**-anchored resin. This strategy allows us to arylate selective binding partners, which are not amenable for the pull-down anymore so that we detect only non-selective interactors. Then, the difference between the normal and the competitive pull-down reveals selective binding partners. Since we expected only covalently bound proteins to be attached to the resin after chemoselective arylation, we performed the proteolytic digestion directly on the beads. After subsequent nano liquid chromatography tandem mass spectrometry (nLC-MS/MS)-based proteomic analysis and evaluation, the selective potential interactors were ranked by means of their enrichment efficiency and significance of interaction as calculated from the normal and competitive pull-down (Fig. 4B). A total of 2833 proteins were identified in the pull-down from the whole cell lysate of SW480 cancer cells. Out of these, just a few stood out as potential selective interactors, either due to the enrichment factor, including Nanos homolog 1 (NANOS1) and guanine nucleotide exchange factor VAV2, or due to the significance, including glucose-6-phosphate 1-dehydrogenase (G6PD) and guanine deaminase (GDA).

Strikingly, we identified the selenoprotein thioredoxin reductase 1 (TXNRD1) as the most prominent selective interactor based on enrichment and significance (Fig. 4B). TXNRD1 is a key player in the maintenance of the intracellular redox homeostasis within the *thioredoxin system*, often overexpressed in cancers due to a constitutive activation of the transcription factor and stress sensor NRF2.[36] It is involved in apoptosis induction and has emerged as one of the main targets of cytotoxic gold complexes, including the clinically evaluated auranofin.[37]

Human TXNRDs are homodimers coupled head to tail, each one containing a redox-active CysSec-dyad with neighbouring cysteine and selenocysteine residues in a ligand-accessible active site near the C-terminus responsible for the interaction of the enzyme with various substrates and thioredoxin (TXN) itself.[38] Gold(I)/(III) ions are Lewis acids that can easily access this region, resulting in strong coordination to selenolate (Fig. 1A), while a ligand exchange reaction takes place at the gold centre.[39,40] The so formed gold-selenolate adduct cannot function as a redox-active centre within TXNRD1 and

consequently, the enzyme's activity is inhibited, eventually inducing pro-apoptotic signalling. Since TXNRD1 contains a selenocysteine, this raised the possibility that **Au** may specifically arylate this residue beyond cysteines in human cancer cells.

Therefore, the chemoproteomic approach was expanded to a dose-dependent competition experiment to verify the interaction with TXNRD1 and assess the potency of interaction. This is achieved by titrating **Au** at increasing concentrations (between 0.096 µM and 60 µM) in the competitive pull-down.[29] Once more, TXNRD1 was verified as an interactor of **Au** and showed a clear dose-dependent profile. However, in contrast to earlier observations,[29] we evidenced an unusual interaction profile suggesting that arylation of TXNRD1 by **Au** involves a second binding site. A 2 : 1 binding stoichiometry between **Au** and TXNRD1 is indicated by the apparent enrichment of TXNRD1 after the first arylation step with a maximum at 2.4 µM and a complete competition at 60 µM (Fig. 4C). The catalytic CysSec-dyad of TXNRD1 potentially allows for two arylation events to occur. Compound **Au** seems to interact similarly with peroxiredoxin 4 (PRDX4), but only at the highest tested concentrations. PRDX4 is thus, an unlikely target at pharmacologically relevant concentrations. Noteworthy, we did not observe other proteins with a dose-dependent profile in the tested concentration range.

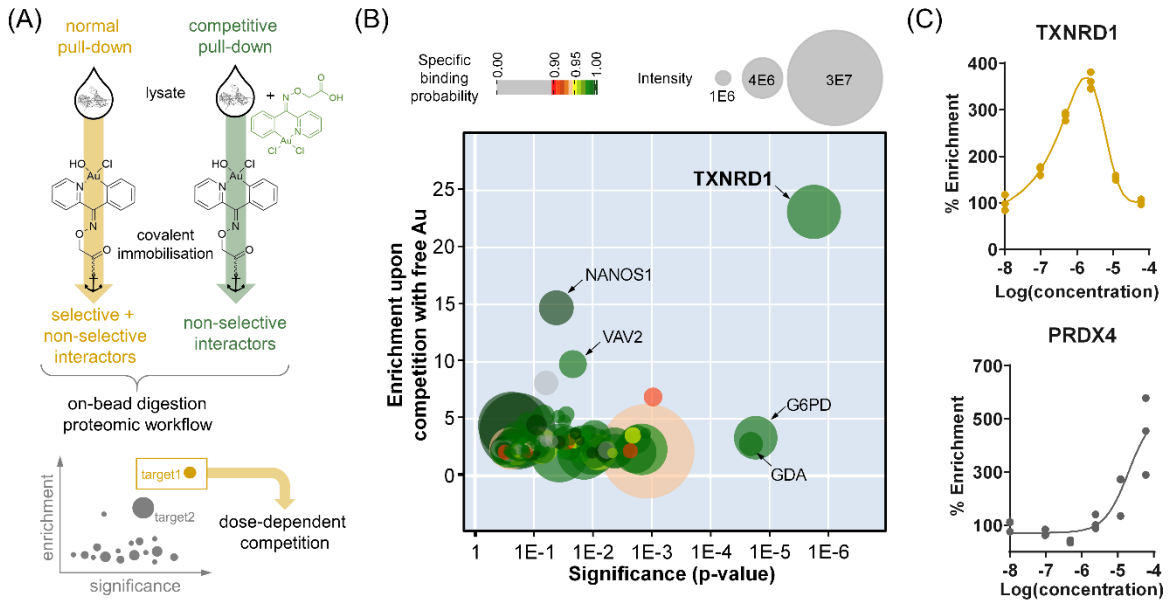

Figure 4. Target identification of immobilised Au using chemoproteomics. (**A**) **Au** was immobilised on amine sepharose beads. Native protein cell lysates of SW480 cancer cells were prepared and either directly incubated with the immobilised probe (normal pull-down) or pre-treated with free **Au** (12 µM, competitive pull-down). (**B**) Differential analysis of the normal and competitive pull-down experiments revealed selective binding to thioredoxin reductase 1 (TXNRD1) from the native protein whole cell lysate of SW480 cancer cells. (**C**) Dose-dependent titration with free **Au** at 0, 96 nM, 480 nM, 2.4 µM, 12 µM and 60 mM

revealed dose-dependent binding affinity only for TXNRD1 and peroxiredoxin 4 (PRDX4). The unusual titration curve indicates bis-arylation of TXNRD1 by **Au** probably at the CysSec-dyad.

Characterisation of Au-mediated arylation of the catalytic CysSec-dyad on TXNRD1

The peculiar reactivity of **Au** towards TXNRD1 in the pull-down suggested the catalytic CysSec-dyad as a likely site of interaction and potentially enabling bis-adduct formation to occur. To characterise the arylation sites, **Au** was reacted with TXNRD1 in a cell-free experiment at 1 : 1 and 5 : 1 molar ratios and incubated for 24 h. Afterwards, TXNRD1 from the reaction mixture was directly proteolytically digested in solution and again analysed by nLC-MS/MS similar to the chemoproteomic experiments. To automatically detect modified peptides of TXNRD1 using MaxQuant (Version 1.6.3.4), arylation and carbamidomethylation had to be customised as variable modifications on cysteine and selenocysteine. The experiment revealed a total of 73% covered protein sequence of TXNRD1 by detecting 51 individual peptides, including the C-terminal peptide that contains the catalytic CysSec-dyad (Fig. 5A). The latter contained the sequence RSGASILQAGCUG (*m/z* 692.7775 (z = 2), m_{theor} = 692.7810) and showed a retention time (RT) of 28.2 min in this experimental setup (Fig. 5B). Interestingly, already at a 1 : 1 molar ratio, two distinct signals for mono-arylation (*m/z* 791.3072 (z = 2), m_{theor} = 791.3058) were observed with RTs of 39.9 min and 40.3 min, respectively. This indicated the presence of two distinct arylation sites on this peptide. Additionally, a bis-arylation product was observed (*m/z* 593.5517 (z = 3), m_{theor} = 593.5551) at RT = 49.1 min substantiating the possibility of two different binding sites on this peptide. These signals increased further when analysing the reaction between **Au** and TXNRD1 at a 5 : 1 molar ratio. The isotopic patterns of the different adducts clearly showed the presence of selenium, revealing excellent simulation matches and mass accuracies <5 ppm (Fig. 5C). Despite the presence of ten other free thiol-containing cysteine residues on TXNRD1 and one additional disulfide bridge formed by two cysteines (PDB 2j3n), we did not find other arylation products up to a molar ratio of 5 : 1 indicating that **Au** is highly specific towards the CysSec-dyad in TXNRD1.

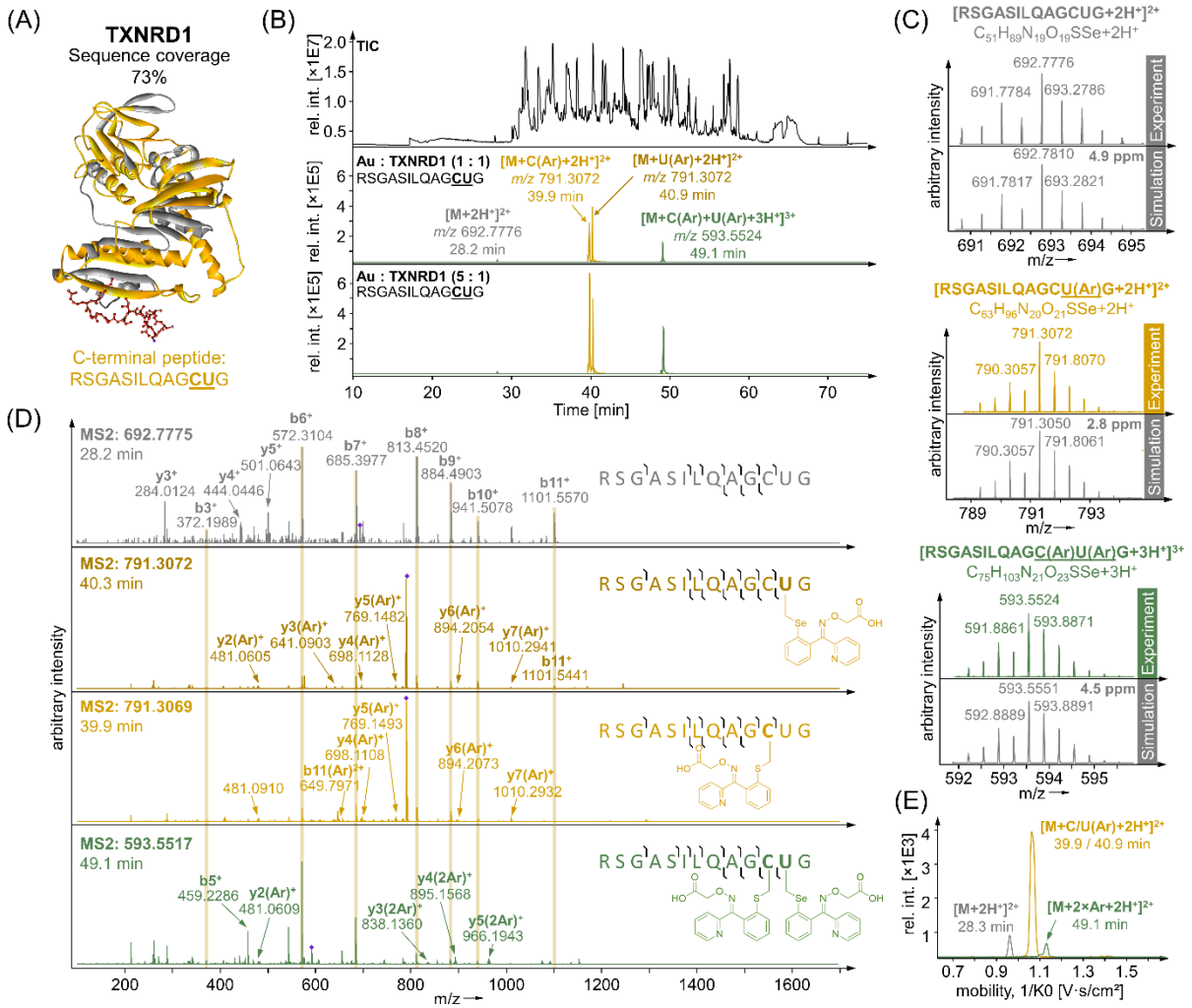

Figure 5. Identification of Au-templated bis-arylation on the CysSec-dyad of TXNRD1. The compound **Au** was reacted at 1 : 1 and 5 : 1 molar ratios with TXNRD1 (5 µg, 2.25 µM) for 24 h in triplicates. A mock reaction containing only the added volume of DMSO without **Au** was also carried out in triplicates. The protein was proteolytically digested and analysed by nLC-MS/MS. (**A**) A total of 51 peptides were detected that covered 73% of the sequence of TXNRD1. (**B**) The chromatograms depict the total ion chromatogram (TIC), as well as the extracted ion chromatograms of the CU-containing C-terminal peptide. The reaction of TXNRD1 with **Au** led to the arylation of the CysSec-dyad on TXNRD1. C- and U-arylations were observed at both molar ratios, as well as bis-arylations. (**C**) The experimental mass signals and theoretical simulations of the isotope patterns of the terminal CU-containing peptide are shown without modification (grey), with mono-arylation (yellow) and with bis-arylation (green) modifications. (**D**) MS/MS experiments of the unmodified and covalently modified CysSec-dyad containing peptide unambiguously identified the location of the arylation sites on C and U. (**E**) The different arylation products of the terminal peptide of TXNRD1 feature distinct ion mobilities that are proportional to their mass.

The four detected mass signals corresponding to the unmodified CysSec-dyad peptide (RT = 28.2 min), the two mono-arylated peptides (RT = 39.9 and 40.3 min) and the bis-arylated peptide (RT = 49.1 min) were individually selected for MS/MS analysis at their respective retention times (Fig. 5D). MS/MS

analysis revealed detailed information about the peptide sequence and the location of the arylation sites. The unmodified peptide was identified with characteristic b– and y-fragments.[41,42] The b_{11}^+ fragment represents an unmodified cysteine, while y_3^+ represents the unmodified C-terminal CUG fragment of this peptide.

Interestingly, the b-fragments remained similar for the mono-arylated product at 40.3 min, including the b_{11}^+ fragment. In contrast, the detected y-fragments indicated an arylation product and the arylated y_2^+ fragment [$y_2(Ar)^+$] provided direct proof of selenocysteine arylation on TXNRD1. The second mono-arylation product eluting at RT = 39.3 min did not feature the unmodified b_{11}^+ ion.

Indeed, the lack of the b_{11}^+ ion and the detection of an arylated b_{11}^+ ion ($b_{11}(Ar)^+$) suggests that this species corresponds to a cysteine arylation product. Finally, the MS/MS spectrum of the bis-arylation product eluting at 49.1 min revealed very different fragment signals that supported simultaneous cysteine and selenocysteine arylation. For example, the fragments $y_2(Ar)^+$ and $y_3(2Ar)^+$ clearly evidenced bis-arylation of the CysSec-dyad of TXNRD1. Other arylation sites on TXNRD1 were not observed. Such terminal peptide was neither observed unmodified or arylated in the proteome profiling experiments of SW480 cancer cells treated with **Au** (data not shown).

In addition to their characteristic *m/z*-ratios, retention times and fragmentation spectra, the CysSec-dyad containing peptides all featured distinct ion mobilities and showed higher mobilities for species with larger molecular mass (Fig. 5E).

Effects of Au-mediated covalent targeting of TXNRD1 on the Proteome of SW480 cancer cells

Finally, we evaluated the effects of **Au** treatment on the protein abundance levels of SW480 cancer cells by proteome profiling. For this purpose, SW480 cancer cells were treated with **Au** at sub-cytotoxic concentration (12 µM) for 24 h. The cytoplasmic (CYT) and nuclear (NE) protein fractions were separately processed and analysed according to our proteomics workflow using a data-dependent label free quantification strategy.[43] A total of 4347 protein groups were identified. As shown in Fig. 6A, the correlation among biological replicates was typically around 0.85, as exemplified for two **Au**-treated NE fractions. This led to a clear separation of the proteome profiles of the different conditions, as revealed by the principal component analysis (SI, Fig. S8A).

Therein, the controls, **Au**-treatments, as well as CYT and NE fractions were clearly separated, while the intra-condition replicates were clustered together indicating homogeneous treatment effects. Of the

total number of proteins, 117 and 465 protein groups were significantly regulated in the CYT and NE fraction, respectively (SI, Fig. S8B). Statistical significance was calculated using multiple testing corrected p-values based on 5% false-discovery rate (FDR = 0.05 and S0 = 0.1). **Au**-treatment induced heme oxygenase 1 (HMOX1), sulfiredoxin 1 (SRXN1) and heat shock 70 kDa protein 1A (HSPA1A) considerably in the CYT fraction. The induction of HSPA1A is also depicted in the profile plot highlighting the stability of the entire experiment (Fig. 6B). Although **Au** targets TXNRD1, the protein was not found to be significantly regulated at this sub-cytotoxic treatment (Fig. 6B). The second putative binding partner PRXD4 was present at similar abundance and was also not significantly regulated (Fig. 6C). Selenoprotein expression is known to depend on selenium availability.[44,45] **Au** treatment led to the significant down-regulation of the three detected selenoproteins glutathione peroxidase 1 (GPX1), glutathione peroxidase 4 (GPX4) and the mitochondrial protein adenylyltransferase SelO (SELO), which may be explained by the reduction of the available intracellular selenium-pool by the **Au**-treatment. Selenium deficiency is known to lead to selenoprotein truncation, as a consequence of misinterpreting UGA as a normal stop codon instead of a codon for selenocysteine, and subsequent degradation by CRL2 and the proteasomal system.[46] Probably, TXNRD1 remains unaffected because selenocysteine is located close to the *C*-terminus.

The global effects of **Au** on the proteome of SW480 cancer cells were further illustrated by grouping the significantly regulated proteins according to gene ontology cellular compartments and biological processes, and plotting their summed fold-changes according to CYT and NE fractions. In parallel to the fluorescence-based cellular uptake, we found cytosolic, nuclear and nucleolar proteins to be the mainly disturbed cellular compartments (Fig. 6D). Additionally, there seems to be a minor impact on mitochondria. The biological processes revealed the induction of NRF2 target genes as the strongest perturbation in both CYT and NE (Fig. 6E, SI Table S1).[36] This is accompanied by induction of heat shock proteins and an ER-based unfolded protein response (UPR), which is indicative of proteotoxic stress possibly due to non-specific **Au**-templated arylation reactions in these cells. Similarly to a previously reported Au(I) bis-N-heterocyclic carbene compound,[43] the proteasome was observed to be translocated to the nucleus, which may be the result of nuclear stress responses. This implies that proteasomal translocation may be the consequence of the presence of a protein-reactive compound in the nucleus. These findings are supported by an analogous pathway representation with similar findings (SI, Fig. S8C).

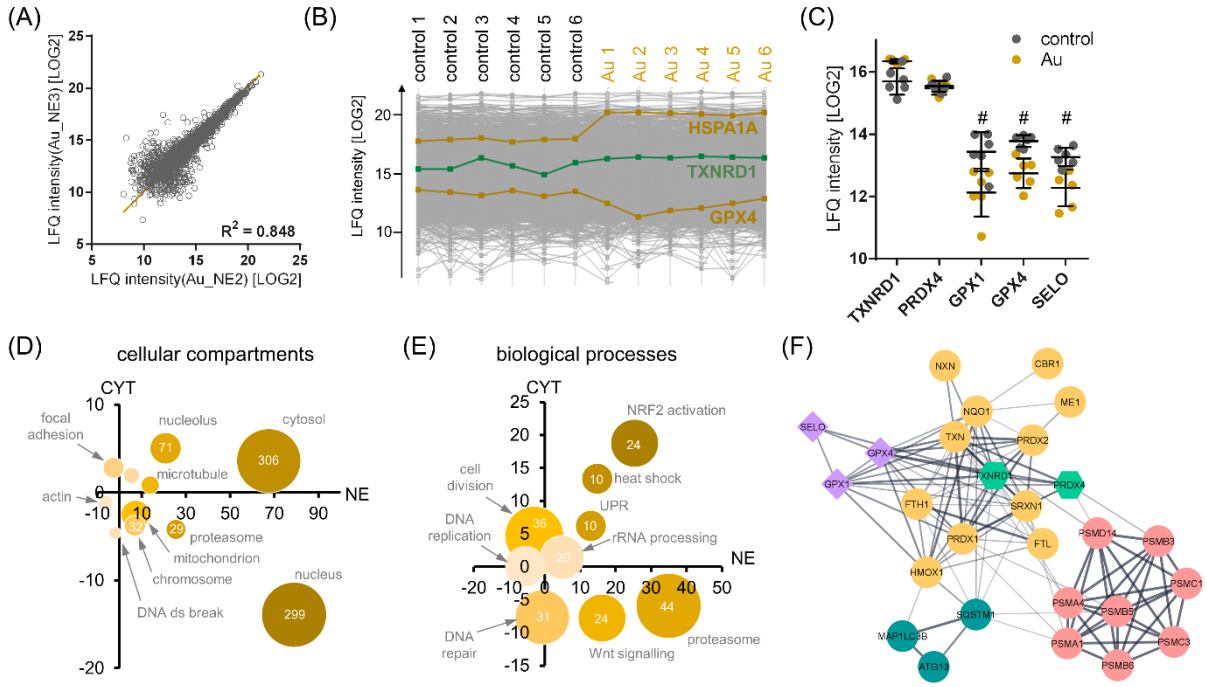

Figure 6. Effects of targeting TXNRD1 by Au in SW480 cancer cells. SW480 cancer cells were treated with half-EC_{50} concentration of **Au** for 24 h. The protein content was fractionated into cytoplasmic (CYT) and nuclear (NE) extracts and processed according to a LC-MS/MS proteomics workflow. Control and treated samples were performed in hexuplicates. (**A**) The scatter plot shows the distribution of the detected proteins according to the intensity of two biological replicates of nuclear extracts of **Au**-treated cells. (**B**) The profile plot highlights the stability of protein abundance within the biological replicates by visualising the label-free quantification (LFQ) intensities of HSPA1A (significantly upregulated), TXNRD1 (not regulated) and GPX4 (significantly down-regulated). (**C**) While the selenoproteins GPX1, GPX4 and SELO are significantly down-regulated upon treatment, the potential targets TXNRD1 and PRDX4 are not. Significant protein regulations (# = p-value<0.05) were obtained after multiple testing correction using a false-discovery rate (FDR) of 0.05 and S0 = 0.1. (**D**) The significantly regulated proteins were grouped according to cellular compartment and visualised by plotting the summed LOG2(fold-changes) according to CYT and NE. The size of the bubbles represents the number of regulated proteins in the group. (**E**) The regulated proteins were also grouped according to biological processes and similarly visualised. (**F**) The target-response network depicts the regulated proteins around the potential binding partners TXNRD1 and PRDX4 indicates effects on redox homeostasis (gold circles), protein degradation *via* the proteasome (rose circles), selenoproteins (purple diamonds) and autophagy (turquois circles). Circle = upregulated protein, diamond = down-regulated protein, hexagon = not regulated. Significantly regulated proteins were multiple testing corrected using a 5% FDR and S0 = 0.1.

As highlighted by the target-response network, which depicts the significantly regulated proteins in the protein neighbourhood of TXNRD1 and PRDX4 (Fig. 6F), the redox balance of SW480 cancer cells was clearly affected by the **Au**-templated targeting of TXNRD1. These proteins are located in the centre of the network surrounded by a cluster of upregulated NRF2-derived redox proteins (yellow, *e.g.* HMOX1,

SRXN1, TXN, peroxiredoxin 1 (PRDX1) and NAD(P)H dehydrogenase [quinone] 1 (NQO1) etc.). The down-regulated selenoproteins GPX1, GPX4 and SELO (purple) are directly connected to these redox proteins and TXNRD1, as well. Autophagy-related proteins (turquoise, *e.g.* sequestosome 1 (SQSTM1) and autophagy-related protein 13 (ATG13)) and proteasomal proteins (rose, *e.g.* proteasomal subunit alpha type-1 (PSMA1), alpha type-4 (PSMA4), beta type-5 (PSMB5) etc.), which digest irreversibly damaged proteins, were also upregulated. Therefore, **Au**-templated covalent targeting of mainly TXNRD1 leads to a substantial effect on the redox balance of the SW480 cancer cells. As a consequence, cells try to cope with this challenge by strongly inducing an NRF2-stress response and translocating the proteasome to the nuclear compartment.

To functionally evaluate the dependence of survival of **Au**-treated SW480 cancer cells on the induction of the NRF2 stress response, we tested for synergism[47] by co-treatment with the HMOX1-inhibitor OB-24.[48] HMOX1 was the most strongly upregulated expression product of the NRF2 target genes upon treatment with **Au** in both CYT and NE fractions (SI, Fig. S8C). Interestingly, HMOX1 protects cells from oxidative stress and has anti-apoptotic properties.[49] After determining the individual EC_{50}-profiles of **Au** and OB-24 in SW480 cancer cells after 72 h incubation, combination treatments were performed according to 0, EC_{10}, EC_{25}, EC_{50}, EC_{75} and EC_{90}-concentrations, giving a total of 36 combinations. At EC_{75} concentrations of **Au**, a strong synergism (δ-score >30) was observed with EC_{10} and EC_{25} concentrations of OB-24 (SI, Fig. S9). This verified the dependence of SW480 cancer cells on inducing the NRF2-stress response to cope with the TXNRD1-targeting ability of **Au**.

CONCLUSIONS

Here, we successfully assessed that C^N-cyclometalated gold(III) complexes can perform bioorthogonal post-translational modifications of thiols and selenols. Chemoproteomic studies highlighted TXNRD1 as one of the main direct target proteins for **Au**-templated arylation, featuring the high enrichment efficiency and significance of interaction in pull-down experiments in whole cell lysates of SW480 cells. Furthermore, nLC-MS/MS experiments with the isolated TXNRD1 revealed the selectivity of **Au**-templated arylation towards the C-terminal CysSec-dyad. Despite the fact that the peptide sequence contains other possible cysteine binding partners, mono- and bis-Cys/Sec arylation was limited to the CysSec-dyad of the enzyme active site, even with an excess of **Au**. A fluorescent derivative of the title compound, **Au-Fluo**, enabled investigation by fluorescence microscopy, showing that the compound can be efficiently taken up by cancer cells and is evenly distributed with a slight preference for the nuclei.

SW480 cancer cells were treated with **Au** at sub-cytotoxic concentrations to evaluate cellular stress responses against the perturbation. Although **Au** did not influence TXNRD1 expression, significant proteome changes were found associated with maintaining the cellular redox balance. These changes were characterised by the downregulation of the detected selenoproteins (*e.g.* GPX1, GPX4, SELO) mainly involved in the ROS detoxification, and the induction of NRF2-derived redox proteins regulating the expression of antioxidant proteins, autophagy-related proteins, as well as proteins involved in the ubiquitin-proteasome protein degrading system. Noteworthy, this study confirms TXNRD1 as a main target of the C^N-cyclometalated gold(III) complex **Au**, acting *via* selenocysteine/cysteine arylation in the protein active site. This metal-templated MoA, fostering the formation of C–S(Se) bonds under physiological conditions, can be further exploited in the design of anticancer organogold compounds acting *via* selective covalent modification of (onco-)proteins. Furthermore, recent reports on the *in vitro*/*in vivo* anticancer effects of this family of C^N-cyclometalated gold(III) complexes[50-54] could be revisited to consider this bioorthogonal reactivity as part of the compounds' MoA.

AUTHOR CONTRIBUTIONS

MP, SRT and RB synthesised and characterised the compounds. MP and SRT investigated stability and reactivity. MP and RB evaluated fluorescence properties. LS and CS performed cell culture experiments. LS performed coupling reactions. LS and GDF carried out cellular accumulation experiments. LS and CS performed proteomic and chemoproteomic experiments. LS and AB characterised protein arylation. AB acquired and searched proteomic data. AC evaluated synthesis and fluorescence data. LS, CS, AB and TM evaluated proteomic data. CG, AC and SMM supervised the study. LS, CS, AC and SMM wrote the initial manuscript draft, which was edited and approved by all authors.

CONFLICT OF INTEREST

There are no conflicts to declare.

ACKNOWLEDGEMENTS

The authors are grateful to the Core Facility for Mass Spectrometry, the Core Facility Multimodal Imaging (Faculty of Chemistry, University of Vienna) and the Joint Metabolome Facility (University of Vienna and

Medical University of Vienna), which are all members of the Vienna Life-Science Instruments (VSLI). S.M.M acknowledges financial support from the Austrian Science Fund (P33238-N). S.R.T. acknowledges TUM Global Postdoc Fellowship Scheme for funding.

DATA AVAILABILITY

The mass spectrometry proteomics data have been deposited to the ProteomeXchange Consortium via the PRIDE partner repository with the dataset identifier PXD044971 (pull-down) and PXD044966 (profiling).

REFERENCES

1. G. Moreno-Alcántar, P. Picchetti and A. Casini, Gold complexes in anticancer therapy: From new design principles to particle-based delivery systems, *Angew. Chem. Int. Ed.*, 2023, **62**, e202218000.
2. M. Mora, M. C. Gimeno and R. Visbal, Recent advances in gold–NHC complexes with biological properties, *Chem. Soc. Rev.*, 2019, **48**, 447-462.
3. A. Casini, R. Wai-Yin Sun and I. Ott, in *Metallo-Drugs: Development and Action of Anticancer Agents*, De Gruyter, 2018, DOI: 10.1515/9783110470734-007, pp. 199-218.
4. S. Yue, M. Luo, H. Liu and S. Wei, Recent advances of gold compounds in anticancer immunity, *Front. Chem.*, 2020, **8**, 543.
5. C. Nardon, G. Boscutti and D. Fregona, Beyond platinums: Gold complexes as anticancer agents, *Anticancer Res.*, 2014, **34**, 487-492.
6. C. Schmidt and A. Casini, in *Comprehensive Organometallic Chemistry IV*, Elsevier, 2022, vol. 1-15, pp. 297-313.
7. B. Bertrand, L. Stefan, M. Pirrotta, D. Monchaud, E. Bodio, P. Richard, P. Le Gendre, E. Warmerdam, M. H. de Jager, G. M. M. Groothuis, M. Picquet and A. Casini, Caffeine-based gold(I) N-heterocyclic carbenes as possible anticancer agents: Synthesis and biological properties, *Inorg. Chem.*, 2014, **53**, 2296-2303.
8. C. Kaußler, D. Wragg, C. Schmidt, G. Moreno-Alcántar, C. Jandl, J. Stephan, R. A. Fischer, S. Leoni, A. Casini and R. Bonsignore, “Dynamical docking” of cyclic dinuclear Au(I) bis-N-heterocyclic complexes facilitates their binding to G-quadruplexes, *Inorg. Chem.*, 2022, **61**, 20405-20423.
9. M. Martínez-Calvo and J. L. Mascareñas, Organometallic catalysis in biological media and living settings, *Coord. Chem. Rev.*, 2018, **359**, 57-79.
10. K.-C. Tong, C.-N. Lok, P.-K. Wan, D. Hu, Y. M. E. Fung, X.-Y. Chang, S. Huang, H. Jiang and C.-M. Che, An anticancer gold(III)-activated porphyrin scaffold that covalently modifies protein cysteine thiols, *Proc. Natl. Acad. Sci.*, 2020, **117**, 1321-1329.
11. K. Tsubokura, K. K. Vong, A. R. Pradipta, A. Ogura, S. Urano, T. Tahara, S. Nozaki, H. Onoe, Y. Nakao, R. Sibgatullina, A. Kurbangalieva, Y. Watanabe and K. Tanaka, In vivo gold complex catalysis within live mice, *Angew. Chem. Int. Ed.*, 2017, **56**, 3579-3584.
12. S. R. Thomas and A. Casini, Gold compounds for catalysis and metal-mediated transformations in biological systems, *Curr. Opin. Chem. Biol.*, 2020, **55**, 103-110.
13. K. K. Kung, H. M. Ko, J. F. Cui, H. C. Chong, Y. C. Leung and M. K. Wong, Cyclometalated gold(III) complexes for chemoselective cysteine modification via ligand controlled C-S bond-forming reductive elimination, *Chem. Commun.*, 2014, **50**, 11899-11902.
14. R. E. F. de Paiva, Z. Du, D. H. Nakahata, F. A. Lima, P. P. Corbi and N. P. Farrell, Gold-catalyzed C-S aryl-group transfer in zinc finger proteins, *Angew. Chem. Int. Ed.*, 2018, **57**, 9305-9309.
15. S. R. Thomas, R. Bonsignore, J. Sánchez Escudero, S. M. Meier-Menches, C. M. Brown, M. O. Wolf, G. Barone, L. Y. P. Luk and A. Casini, Exploring the chemoselectivity towards cysteine arylation by cyclometallated Au(III) compounds: New mechanistic insights, *ChemBioChem*, 2020, **21**, 3071-3076.

16. M. N. Wenzel, R. Bonsignore, S. R. Thomas, D. Bourissou, G. Barone and A. Casini, Cyclometalated Au(III) complexes for cysteine arylation in zinc finger protein domains: Towards controlled reductive elimination, *Chem. Eur. J.*, 2019, **25**, 7628-7634.
17. C. Schmidt, M. Zollo, R. Bonsignore, A. Casini and S. M. Hacker, Competitive profiling of ligandable cysteines in Staphylococcus aureus with an organogold compound, *Chem. Commun.*, 2022, **58**, 5526-5529.
18. K.-C. Tong, D. Hu, P.-K. Wan, C.-N. Lok and C.-M. Che, Anticancer gold(III) compounds with porphyrin or N-heterocyclic carbene ligands, *Front. Chem.*, 2020, **8**, 587207.
19. B. Bertrand and A. Casini, A golden future in medicinal inorganic chemistry: The promise of anticancer gold organometallic compounds, *Dalton Trans.*, 2014, **43**, 4209-4219.
20. L. Skos, Y. Borutzki, C. Gerner and S. M. Meier-Menches, Methods to identify protein targets of metal-based drugs, *Curr. Opin. Chem. Biol.*, 2023, **73**, 102257.
21. H. Wang, Y. Zhou, X. Xu, H. Li and H. Sun, Metalloproteomics in conjunction with other omics for uncovering the mechanism of action of metallodrugs: Mechanism-driven new therapy development, *Curr. Opin. Chem. Biol.*, 2020, **55**, 171-179.
22. Y. Zhou, H. Li and H. Sun, Metalloproteomics for biomedical research: methodology and applications, *Annu. Rev. Biochem.*, 2022, **91**, 449-473.
23. A. Casini, A. Vessières and S. M. Meier-Menches, *Metal-based anticancer agents*, Royal Society of Chemistry, 2019.
24. S. M. Meier, C. Gerner, B. K. Keppler, M. A. Cinellu and A. Casini, Mass spectrometry uncovers molecular reactivities of coordination and organometallic gold(III) drug candidates in competitive experiments that correlate with their biological effects, *Inorg. Chem.*, 2016, **55**, 4248-4259.
25. M. Wenzel and A. Casini, Mass spectrometry as a powerful tool to study therapeutic metallodrugs speciation mechanisms: Current frontiers and perspectives, *Coord. Chem. Rev.*, 2017, **352**, 432-460.
26. J. Ha, H. Park, J. Park and S. B. Park, Recent advances in identifying protein targets in drug discovery, *Cell Chem. Biol.*, 2021, **28**, 394-423.
27. S. M. Meier, D. Kreutz, L. Winter, M. H. M. Klose, K. Cseh, T. Weiss, A. Bileck, B. Alte, J. C. Mader, S. Jana, A. Chatterjee, A. Bhattacharyya, M. Hejl, M. A. Jakupec, P. Heffeter, W. Berger, C. G. Hartinger, B. K. Keppler, G. Wiche and C. Gerner, An organoruthenium anticancer agent shows unexpected target selectivity for plectin, *Angew. Chem. Int. Ed.*, 2017, **56**, 8267-8271.
28. B. Neuditschko, A. A. Legin, D. Baier, A. Schintlmeister, S. Reipert, M. Wagner, B. K. Keppler, W. Berger, S. M. Meier-Menches and C. Gerner, Interaction with ribosomal proteins accompanies stress induction of the anticancer metallodrug BOLD-100/KP1339 in the endoplasmic reticulum, *Angew. Chem. Int. Ed.*, 2021, **60**, 5063-5068.
29. B. Neuditschko, A. P. King, Z. Huang, L. Janker, A. Bileck, Y. Borutzki, S. C. Marker, C. Gerner, J. J. Wilson and S. M. Meier-Menches, An anticancer rhenium tricarbonyl targets Fe−S cluster biogenesis in ovarian cancer cells, *Angew. Chem. Int. Ed.*, 2022, **61**, e202209136.
30. S. K. Fung, T. Zou, B. Cao, P.-Y. Lee, Y. M. E. Fung, D. Hu, C.-N. Lok and C.-M. Che, Cyclometalated gold(III) complexes containing N-heterocyclic carbene ligands engage multiple anti-cancer molecular targets, *Angew. Chem. Int. Ed.*, 2017, **56**, 3892-3896.
31. P.-K. Wan, K.-C. Tong, C.-N. Lok, C. Zhang, X.-Y. Chang, K.-H. Sze, A. S. T. Wong and C.-M. Che, Platinum(II) N-heterocyclic carbene complexes arrest metastatic tumor growth, *Proc. Natl. Acad. Sci.*, 2021, **118**, e2025806118.
32. M. Prechova, Z. Adamova, A.-L. Schweizer, M. Maninova, A. Bauer, D. Kah, S. M. Meier-Menches, G. Wiche, B. Fabry and M. Gregor, Plectin-mediated cytoskeletal crosstalk controls cell tension and cohesion in epithelial sheets, *J. Cell Biol.*, 2022, **221**, e202105146.
33. H. Wang, L. Hu, H. Li, Y.-T. Lai, X. Wei, X. Xu, Z. Cao, H. Cao, Q. Wan, Y.-Y. Chang, A. Xu, Q. Zhou, G. Jiang, M.-L. He and H. Sun, Mitochondrial ATP synthase as a direct molecular target of chromium(III) to ameliorate hyperglycaemia stress, *Nat. Commun.*, 2023, **14**, 1738.
34. V. Sourjik, H. Wang, A. Yan, Z. Liu, X. Yang, Z. Xu, Y. Wang, R. Wang, M. Koohi-Moghadam, L. Hu, W. Xia, H. Tang, Y. Wang, H. Li and H. Sun, Deciphering molecular mechanism of silver by integrated omic approaches enables enhancing its antimicrobial efficacy in E. coli, *PLOS Biol.*, 2019, **17**, e3000292.
35. Y. Wang, L. Hu, F. Xu, Q. Quan, Y.-T. Lai, W. Xia, Y. Yang, Y.-Y. Chang, X. Yang, Z. Chai, J. Wang, I. K. Chu, H. Li and H. Sun, Integrative approach for the analysis of the proteome-wide response to bismuth drugs in Helicobacter pylori, *Chem. Sci.*, 2017, **8**, 4626-4633.
36. M. Dodson, M. R. de la Vega, A. B. Cholanians, C. J. Schmidlin, E. Chapman and D. D. Zhang, Modulating NRF2 in disease: Timing Is everything, *Annu. Rev. Pharm. Tox.*, 2019, **59**, 555-575.

37. Y. Lu, X. Ma, X. Chang, Z. Liang, L. Lv, M. Shan, Q. Lu, Z. Wen, R. Gust and W. Liu, Recent development of gold(I) and gold(III) complexes as therapeutic agents for cancer diseases, *Chem. Soc. Rev.*, 2022, **51**, 5518-5556.
38. K. Fritz-Wolf, S. Kehr, M. Stumpf, S. Rahlfs and K. Becker, Crystal structure of the human thioredoxin reductase–thioredoxin complex, *Nat. Commun.*, 2011, **2**, 1382.
39. A. Bindoli, M. P. Rigobello, G. Scutari, C. Gabbiani, A. Casini and L. Messori, Thioredoxin reductase: A target for gold compounds acting as potential anticancer drugs, *Coord. Chem. Rev.*, 2009, **253**, 1692-1707.
40. A. Casini, A. Guerri, C. Gabbiani and L. Messori, Biophysical characterisation of adducts formed between anticancer metallodrugs and selected proteins: New insights from X-ray diffraction and mass spectrometry studies, *J. Inorg. Biochem.*, 2008, **102**, 995-1006.
41. S. M. Meier, Y. O. Tsybin, P. J. Dyson, B. K. Keppler and C. G. Hartinger, Fragmentation methods on the balance: Unambiguous top–down mass spectrometric characterization of oxaliplatin–ubiquitin binding sites, *Anal. Bioanal. Chem.*, 2011, **402**, 2655-2662.
42. C. G. Hartinger, M. Groessl, S. M. Meier, A. Casini and P. J. Dyson, Application of mass spectrometric techniques to delineate the modes-of-action of anticancer metallodrugs, *Chem. Soc. Rev.*, 2013, **42**, 6186-6199.
43. S. M. Meier-Menches, B. Neuditschko, K. Zappe, M. Schaier, M. C. Gerner, K. G. Schmetterer, G. Del Favero, R. Bonsignore, M. Cichna-Markl, G. Koellensperger, A. Casini and C. Gerner, An organometallic gold(I) bis-N-heterocyclic carbene complex with multimodal activity in ovarian cancer cells, *Chem. Eur. J.*, 2020, **26**, 15528-15537.
44. L. Schomburg and U. Schweizer, Hierarchical regulation of selenoprotein expression and sex-specific effects of selenium, *Biochim. Biophys. Acta*, 2009, **1790**, 1453-1462.
45. Z. Touat-Hamici, A.-L. Bulteau, J. Bianga, H. Jean-Jacques, J. Szpunar, R. Lobinski and L. Chavatte, Selenium-regulated hierarchy of human selenoproteome in cancerous and immortalized cells lines, *Biochim. Biophys. Acta*, 2018, **1862**, 2493-2505.
46. H.-C. Lin, S.-C. Ho, Y.-Y. Chen, K.-H. Khoo, P.-H. Hsu and H.-C. S. Yen, CRL2 aids elimination of truncated selenoproteins produced by failed UGA/Sec decoding, *Science*, 2015, **349**, 91-95.
47. A. Ianevski, A. K. Giri and T. Aittokallio, SynergyFinder 3.0: An interactive analysis and consensus interpretation of multi-drug synergies across multiple samples, *Nucleic Acids Res.*, 2022, **50**, W739-W743.
48. M. A. Alaoui-Jamali, T. A. Bismar, A. Gupta, W. A. Szarek, J. Su, W. Song, Y. Xu, B. Xu, G. Liu, J. Z. Vlahakis, G. Roman, J. Jiao and H. M. Schipper, A novel experimental heme oxygenase-1–targeted therapy for hormone-refractory prostate cancer, *Cancer Res.*, 2009, **69**, 8017-8024.
49. I. Petrache, L. E. Otterbein, J. Alam, G. W. Wiegand and A. M. K. Choi, Heme oxygenase-1 inhibits TNF-α-induced apoptosis in cultured fibroblasts, *Am. J. Physiol. Lung Cell. Mol. Physiol.*, 2000, **278**, L312-L319.
50. M. V. Babak, K. R. Chong, P. Rapta, M. Zannikou, H. M. Tang, L. Reichert, M. R. Chang, V. Kushnarev, P. Heffeter, S. M. Meier-Menches, Z. C. Lim, J. Y. Yap, A. Casini, I. V. Balyasnikova and W. H. Ang, Interfering with metabolic profile of triple-negative breast cancers using rationally designed metformin prodrugs, *Angew. Chem. Int. Ed.*, 2021, **60**, 13405-13413.
51. A. L. de Andrade Querino, A. M. de Sousa, S. R. Thomas, G. M. de Lima, D. Dittz, A. Casini, R. L. do Monte-Neto and H. Silva, Organogold(III)-dithiocarbamate compounds and their coordination analogues as anti-tumor and anti-leishmanial metallodrugs, *J. Inorg. Biochem.*, 2023, **247**, 112346.
52. J. H. Kim, S. Ofori, S. Parkin, H. Vekaria, P. G. Sullivan and S. G. Awuah, Anticancer gold(III)-bisphosphine complex alters the mitochondrial electron transport chain to induce in vivo tumor inhibition, *Chem. Sci.*, 2021, **12**, 7467-7479.
53. B. Bertrand, S. Spreckelmeyer, E. Bodio, F. Cocco, M. Picquet, P. Richard, P. Le Gendre, C. Orvig, M. A. Cinellu and A. Casini, Exploring the potential of gold(III) cyclometallated compounds as cytotoxic agents: variations on the C^N theme, *Dalton Trans.*, 2015, **44**, 11911-11918.
54. E. Abás, A. Bellés, A. Rodríguez-Diéguez, M. Laguna and L. Grasa, Selective cytotoxicity of cyclometalated gold(III) complexes on Caco-2 cells is mediated by G2/M cell cycle arrest, *Metallomics*, 2021, **13**, mfab034.